Published online 3 December 2007

Nucleic Acids Research, 2008, Vol. 36, No. 2 ***607–615***
doi:10.1093/nar/gkm672

Escherichia coli low-copy-number plasmid R1 centromere *parC* forms a U-shaped complex with its binding protein ParR

C. Hoischen[1], M. Bussiek[2], J. Langowski[2] and S. Diekmann[1,*]

[1]Molecular Biology, FLI, Leibniz-Institute for Age Research, Beutenbergstrasse 11, D-07745 Jena, Germany and [2]Division Biophysics of Macromolecules, DKFZ, INF 580, D-69120 Heidelberg, Germany

Received June 21, 2007; Revised August 15, 2007; Accepted August 16, 2007

ABSTRACT

The *Escherichia coli* low-copy-number plasmid R1 contains a segregation machinery composed of *parC*, ParR and *parM*. The R1 centromere-like site *parC* contains two separate sets of repeats. By atomic force microscopy (AFM) we show here that ParR molecules bind to each of the 5-fold repeated iterons separately with the intervening sequence unbound by ParR. The two ParR protein complexes on *parC* do not complex with each other. ParR binds with a stoichiometry of about one ParR dimer per each single iteron. The measured DNA fragment lengths agreed with B-form DNA and each of the two *parC* 5-fold interon DNA stretches adopts a linear path in its complex with ParR. However, the overall *parC*/ParR complex with both iteron repeats bound by ParR forms an overall U-shaped structure: the DNA folds back on itself nearly completely, including an angle of ~150°. Analysing linear DNA fragments, we never observed dimerized ParR complexes on one *parC* DNA molecule (intramolecular) nor a dimerization between ParR complexes bound to two different *parC* DNA molecules (intermolecular). This bacterial segrosome is compared to other bacterial segregation complexes. We speculate that partition complexes might have a similar overall structural organization and, at least in part, common functional properties.

INTRODUCTION

In order to ensure genetic stability, DNA molecules must be evenly distributed among daughter cells after replication. Stable maintenance of bacterial low-copy-number plasmids is ensured by a number of active stabilization loci encoded by the plasmids themselves. These loci can be divided into those that function by killing of plasmid-free segregants (1) and those that actively segregate plasmid copies to daughter cells at cell division, i.e. partitioning loci (*par*). All known plasmid *par* systems operate by determining the intracellular position of their replicon such that, after replication, plasmid copies are transported to each side of the bacterial septal plane where they remain positioned until cell division takes place. Thus, by actively distributing plasmid molecules to cell progeny, the *par* systems ensure faithful plasmid inheritance throughout the bacterial population (2–6).

In general, partitioning loci encode three elements: (i) centromere-like site(s) in the plasmid DNA, (ii) a protein binding to this site and (iii) an ATPase. The *Escherichia coli* plasmid R1 is a large (100 kb) low-copy-number plasmid with its segregation machinery encoded by the *par* operon (7,8) composed of *parC*, *ParR* and *parM* (7). The R1 *par* centromere-like site (*parC*) contains two sets of five 11 bp direct repeats (iterons) separated by a region containing the *par* promoter (9,10). The iterons serve as operator sequences to which ParR binds and represses the promoter (10,11). ParR forms dimers in solution and binds to multiple sites in the *parC* region in a cooperative manner (12). Binding of ParR to *parC* serves to autoregulate expression of the *par* genes as well as to form a nucleoprotein complex for partitioning (9,10). *parM* encodes an actin-like ATPase which assembles into dynamically unstable bipolar filaments (13–16). The ParM protein interacts with the *parC*/ParR complex which stabilizes its filament ends (16). *parC*, ParR and ParM are sufficient to form a bipolar DNA-segregating spindle granting plasmid partitioning (8,16,17).

In eukaryotes (with the exception of *Saccharomyces cerevisiae*), centromere DNA is formed by multi-fold repeats of satellite DNA. Cloned satellite monomers

*To whom correspondence should be addressed. Tel: +49 3641 65 6260; Fax: +49 3641 65 6261; Email: diekmann@fli-leibniz.de
Present address:
M. Bussiek, Biophysical Engineering Group, University of Twente, PO Box 217, NL-7500AE Enschede, The Netherlands.

The authors wish it to be known that, in their opinion, the first two authors should be regarded as joint First Authors.

from higher eukaryotes (18,19) including humans (19,20) as well as yeast centromeric DNA (*S. cerevisiae*; (21)) exhibit anomalously slow migration in polyacrylamide gels indicative of DNA curvature (22–25). Recently, we showed that also *parC* is strongly curved (26). The curvature of the *parC* sequence might support the multiple ParR binding to *parC* and might result in a folded shape of the DNA–protein complex also in bacteria. We thus studied the globular shape of the *parC*/ParR complex by atomic force microscopy (AFM). We identified the ParR multimers binding to the two sets of 5-fold repeated iterons in the *parC* sequence. The protein–DNA complex showed a U-shape folded, but not higher order globular, structure.

The mechanisms of low-copy-number plasmid pairing are still unclear. It is widely assumed that the elements to be partitioned pair before they proceed towards opposite poles of a dividing cell (27,28). Here we show that linear *parC* and ParR of plasmid R1 do not show pairing *in vitro*.

MATERIALS AND METHODS

Bacterial strains and growth conditions

The *E. coli* strain DH5α was used for cloning, construction of vectors and for protein expression. Strain *E. coli* K12 J53 carrying plasmid R1drd19 was purchased from the DSMZ (German collection of microorganisms and cell cultures, Braunschweig, Germany). The strains were cultivated in LB medium (37°C, 200 r.p.m.) or on LB agar plates. If necessary, the media were supplemented with the appropriate antibiotics (29).

Cloning, expression and purification of ParR

DNA cloning procedures were performed using standard methods (29). The coding region of ParR was amplified from plasmid R1drd19 by PCR using as KasI restriction site introducing upstream primer (ParR f) 5′-GGCG CCTGATGATGGACAAGCGCAGAA-3′ and as XhoI restriction site indroducing downstream primer (ParR r) 5′-CTCGAGTTAATTTATTAGCTTCATCGC-3′. The blunt end PCR product was cloned into pCR 4Blunt-TOPO (Invitrogen, Carlsbad, CA, USA) resulting in vector pTOPO-ParR. After verification of the correct DNA sequence pTOPO-ParR was digested by KasI–XhoI. The 362 bp fragment containing the ParR-coding region was cloned into the 3220 bp KasI–XhoI fragment of plasmid pASK-IBA7+ (IBA, Göttingen, Germany). The resulting plasmid pASK7+ParR harboured the promoter P*tet* controlled *ParR* gene fused to an upstream located Strep-tag-II-Xa coding region.

One hundred and fifty millilitre LB medium was inoculated with 3 ml of a DH5α (pASK7+ParR) overnight culture. After 7 h of cultivation on a rotary shaker (220 r.p.m., 28°C) protein expression was induced by addition of anhydrotetracycline (atc) to a final concentration of 0.2 μg/ml. After further 18 h of cultivation, cells were collected by centrifugation (10 000 *g*, 4°C), washed twice in lysis buffer (Tris–HCl 100 mM, NaCl 150 mM, EDTA 1 mM, PMSF 0.2 mM, pH 8.0), resuspended in 2.5 ml lysis buffer and subsequently disrupted by two French press passages (20 000 psi). After two centrifugation steps of the crude extract (20 min at 30 000 *g* and 1 h at 150 000 *g*, 4°C), the final supernatant was applied four times to a 2 ml Strep-Tactin affinity column (IBA) equilibrated with lysis buffer for purification of ParR (Figure 1). The column was washed with 60 ml lysis buffer and eluted four times with 3 ml elution buffer (Tris–HCl 100 mM, NaCl 150 mM, EDTA 1 mM, desthiobiotin 2.5 mM, pH 8.0). Eluate 2 contained almost pure ParR (2 mg/ml). The purified ParR was stored in elution buffer at −20°C. For binding experiments, ParR was dialysed against binding buffer B (Tris–HCl 10 mM, KCl 50 mM, EDTA 1 mM, DTT 1 mM, 0.02% Nonidet P40, pH 7.8) and centrifuged for 1 h at 150 000 *g*.

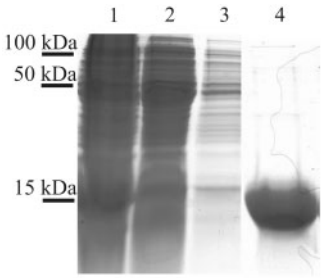

Figure 1. Purification of ParR with Strep-tag Strep-tactin. Coomassie-blue stained SDS–PAGE (17%) of centrifugated crude extract applied to the Strep-tactin column (lane 1), flow through (lane 2), first wash (lane 3) and second eluted fraction (lane 4). Equal volumes of each sample were applied. This allows a direct comparison of the intensities of the stained proteins in the individual lanes.

To verify the data obtained with ParR fused to the Strep-tag, the tag was removed by Factor Xa treatment. ParR was dialysed against a modified Xa buffer (Tris–HCl 50 mM, NaCl 100 mM, Ca_2Cl 5 mM, 10% glycerol, pH 8.0) and incubated with factor Xa (Novagen, Madison, USA) at a final concentration of 80 U/ml according to manufacturer's instructions for 48 h at 27°C. After dialysis against lysis buffer and inactivation of Xa by EDTA and PMSF, the reaction mix was applied to a Strep-Tactin column in order to remove Strep-tag fused ParR. The flow through containing ParR and inactivated Xa was dialysed against buffer B and used for further experiments.

Western blot analysis of the various pellet and supernatant fractions obtained during extract preparation and purification revealed that by far the majority of the expressed protein was located in a soluble form in the high speed supernatant (150 000 *g*).

The expression of a Gst-ParR fusion protein did not result in sufficient material for purification and further analysis.

Protein methods

Proteins of cultures, washed cells, crude extracts, supernatant and pellet fractions were separated by SDS–PAGE (17%) and visualized by Coomassie brilliant blue. For western blot analysis, the gels were electroblotted to polyvinylidene difluoride membranes (Millipore, Bedford, MA, USA). For detection, we used Strep-Tactin conjugated to alkaline phosphatase (IBA) according to the manufacturer's instructions. Proteins were determined by

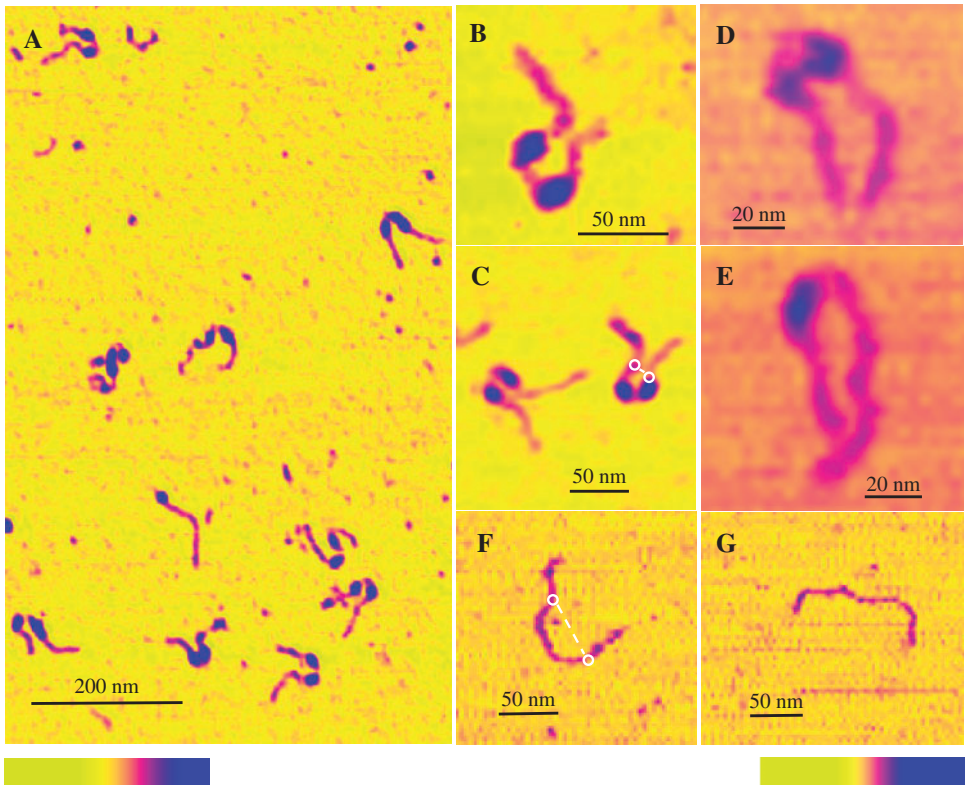

Figure 2. AFM of the *parC*/ParR complexes. (**A**) Representative overview scanned in air. (**B** and **C**) Single complexes in air. (**D**) Single complex in fluid. (**E**) Single complex in fluid with just one protein complex. (**F** and **G**) Single naked DNA fragments in fluid. Left height scale for A–C: 0 nm (yellow)–4 nm (blue); right height scale for D–G: 0 nm (yellow)–8 nm (blue). The length scale is given for each picture by a bar with its length indicated. White circles connected by dashed white lines in C and F represent those positions on the fragments located in a distance of 40 nm from the tips of the DNA arms.

the method of Bradford or were analysed by UV spectroscopy at 280 nm using a calculated molar extinction coefficient of 7210 (±5%).

Preparation of the *parC* containing DNA

For activity assays of the ParR preparations and for AFM analysis of the *parC*/ParR complex, we used a 470 bp BspHI fragment of the pKG330 plasmid asymmetrically carrying the 159 bp *parC* region (Figure 2 in (26)). After BspHI restriction, the 470 bp fragment was separated by agarose gel electrophoresis (1% agarose in TAE buffer), purified by gel extraction (Qiagen, Hilden, Germany) and ethanol precipitation and dissolved to a final concentration of 0.2 µg/µl in TE buffer.

ParR activity assay

ParR activity, i.e. binding of ParR to *parC*, was determined by gel retardation (12). A total of 0.5 µg of the *parC* containing 470 bp BspHI fragment were phosphorylated by terminal transferase according to manufacturer's instructions (NEB, MA, USA) using 60 µCi α-ddATP (3000 Ci/mmol; Amersham Buchler, Buckinghamshire, UK), purified using minielute columns (Qiagen) and resuspended in H_2O. ^{32}P-labelled DNA (2 nM) was incubated with purified ParR (1–1000 nM) for 30 min at room temperature in buffer B. After addition of glycerol to a final concentration of 5%, 10 µl of the sample was loaded on a native 6% polyacrylamide gel (29:1 acrylamide:bisacrylamide; Bio-Rad, USA). Gels were prerun for ~3 h until current and temperature remained constant. Electrophoresis was carried out in 1 × TBE (90 mM Tris–borate, 2 mM Na-EDTA, pH 8.0) at 150 V (8 mA) for ~4 h at room temperature. After the runs, the gels were dried and analysed by phosphoimaging (Storm, USA).

Sample preparation for AFM

Freshly cleaved mica was functionalized with poly-L-lysine (PL, Sigma, Deisenhofen, Germany) to support a secure immobilization of the DNA for the AFM measurements (30). This was done by incubating the mica disc with 30 µl of a 5–10 µg/ml solution of PL and subsequent washing with 4 ml of Millipore water and drying under a nitrogen stream. Then, the 470-bp long *parC* containing fragments were mixed with ParR in 10 µl buffer B to final concentrations of 0.33 µM and up to 20 µM of *parC* and ParR, respectively. If not stated otherwise, experiments were carried out with ParR concentrations of 10 µM. After 15–30 min, the mixture was diluted 30-fold in buffer B and 30 µl of this dilution was immediately placed on the PL-mica. This preparation was used directly for scanning in liquid. For scanning in air, the mica was rinsed carefully with 2 ml of Millipore water after an incubation with the mixture for 1 min and blown dry.

AFM measurements

AFM measurements were done using a Multimode™ (IIIa, Veeco Instruments, Woodbury, New York, USA) operated in tapping mode essentially as described (30). Dried samples were scanned with etched silicon probes (type NHC, Nanosensors, Neuchatel, Switzerland) at drive frequencies of 280–320 kHz and set point of 2.0–2.2 V. Samples in liquid were scanned with sharpened silicon nitride probes (type NP-S) at drive frequencies of 8.0–9.5 kHz and set points of 0.4–0.5 V. Fields of 1×1 to 3×3 μm were scanned at line rates of 1–2 Hz and resolution of 512×512 pixels. The shape of the used tip is specified by the tip end curvature (lower limit of end radius 10 nm) and the tip opening angle (<35°; Veeco Instruments).

Image analysis

AFM images were flattened and 20×20 nm zooms of individual complexes for subsequent analyses were prepared using the Nanoscope IIIa software (version 5.12r3, Veeco Instruments). Heights of naked DNA and of protein complexes bound to DNA were measured using the section analysis tool of the same software package. All other measurements were done with the program ImageJ (version 1.36b, National Institute of Health, Bethesda, USA). To measure the lengths of naked DNA fragments and of DNA complexed with ParR, contours were traced using the freehand line tool. To determine the bending angle of the central DNA region connecting the two ParR complexes, we used the angle tool.

RESULTS

The *parC* fragment is 159 bp in length and organized in two regions each containing a 5-fold repeated sequence motif of 11 bp length with a central intervening region of 39 bp containing the *par* promoter (12). The full *parC* sequence containing the 10 repeats (iterons) is strongly curved (26). This curvature might support ParR binding and the complex formed might show a folded globular shape (28). We studied the *parC*/ParR complex by AFM in order to elucidate the structure of the complex formed only by linearized *parC* and purified ParR with samples neither fixed by cross-linking nor stained by contrasting agents. Using AFM with molecular samples under buffer is one of the most gentle methods to visualize macromolecules.

The *parC* fragment had originally been cloned into the plasmid pKG330 (7). Those parts of the plasmid relevant for complex analysis were verified by sequencing. The gene of the *parC*-binding protein ParR was amplified by PCR using plasmid R1drd19 as template and the sequence was verified. ParR was expressed as a Strep-tag fusion protein in *E. coli* and purified to close homogeneity by affinity chromatography as shown by SDS–polyacrylamide gel-electrophoresis (PAGE) in Figure 1 (lane 4). The purified fusion protein migrated in the gel according to its molecular weight of 15 kDa. In addition, specific recognition of the purified fusion protein by alkaline phosphatase conjugated Strep-Tactin revealed one single protein band of the expected size (data not shown). The binding activity of ParR to *parC* was studied in a gel shift experiment. The 470-bp long *parC* fragment (obtained by digestion of pKG330 with BspH1) was ^{32}P labelled at its ends. This DNA was incubated with the purified Strep-tag ParR fusion protein or, alternatively, with the pure ParR released from its Strep fusion partner by endoproteinase Xa treatment. In both cases, with and without Strep-tag, ParR caused a band shift of *parC* in PAGE. The binding properties obtained for the ParR Strep-tag fusion protein and for ParR without tag were similar, both in agreement with published data (12) (data not shown). Thus, the cloned protein is functionally active.

We analysed *parC* DNA without bound ParR on the AFM surface, which was scanned either directly in the binding buffer (Figure 2F and G, insert Figure 5) or after air drying. In both cases, the DNA molecules could be clearly identified. The DNA diameter was measured in buffer by analysing the peak height. The average of 42 measurements revealed a DNA diameter of 1.6 nm. This value is 80% of the expected value of 2.0 nm, a reduction arising from interactions between sample and the AFM tip. Previously, a DNA diameter of 1.14 nm was measured for DNA under fluid (31). The measured fragment lengths (159.1 ± 4 nm under fluid, 159.4 ± 4 nm in air) agree perfectly with the expected value (157.5 nm) for a 470 bp DNA with a rise per base pair of 0.335 nm.

The ParR protein was incubated with *parC* in a molar ratio of 30:1 up to 60:1 and deposited on the PL–mica. Under these conditions, most of the *parC* DNA molecules are bound by ParR multimers (12). We were not able to analyse by AFM complexes incubated with ratios larger than 60:1 due to the high background caused by unbound protein. The DNA molecules with bound proteins could be clearly identified on the surface images (Figure 2A–E). Mainly we observed two separate binding peaks of spindle-like shape indicating that ParR forms two distinct complexes along the *parC* site. In a few cases, the DNA carried only one such binding peak indicating that the two iteron repeats are loaded with ParR independently from each other. Already a visual inspection of the images suggested that the two ParR deposits were located at specific positions on the DNA fragments as expected for specific binding of ParR to the two *parC* iterons (see subsequently). The size of the ParR complexes was analysed in buffer by measuring the heights, lengths and widths of 61 complexes. For the analyses of length and width, it was necessary to compensate the systemic distortions introduced by the finite width of the AFM tip. We estimated this systemic distortion according to the differences between the measured height (1.6 nm) of the cylindrical DNA (observed heights should be independent of the tip geometry) and the corresponding width (7.1 nm), resulting in a correction value of 5.5 nm. The apparent widening depends on the tip shape (specified by the end radius of curvature and tip opening angle) and the height and shape of the scanned object itself. The heights of DNA and protein were smaller than the tip end radius of curvature to an amount that the opening angle can be neglected. Taking into account the tip geometry, the correction value for the width of the protein complexes

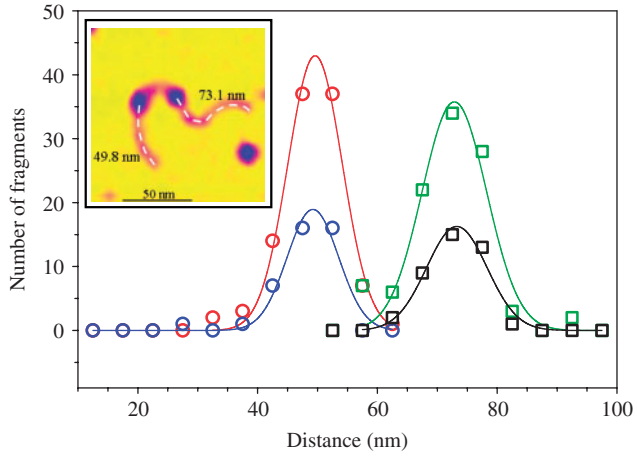

Figure 3. Distances of complex centres to nearest DNA ends. Results of AFM analysis of *parC*/ParR complexes in air and in fluid. For the short DNA arm are shown: (i) the distances of the complex centres to the nearest DNA ends (red circles) measured in air, (ii) the corresponding Gaussian fit as red solid line, (iii) the distances of the complex centres to the nearest DNA end (blue circles) measured in fluid and (iv) the Gaussian fit of these values as blue solid line. The data for the long DNA arm are presented as follows: (i) in air measured values are represented by green squares and (ii) the Gaussian fit is shown by the green solid line, (iii) the data obtained in fluid are symbolized by black squares, whereas (iv) the corresponding Gaussian fit is shown by the black solid line. Insert shows a single *parC*/ParR complex with two ParR complex centres scanned in air. White dashed lines indicate the DNA contour for the distance measurements.

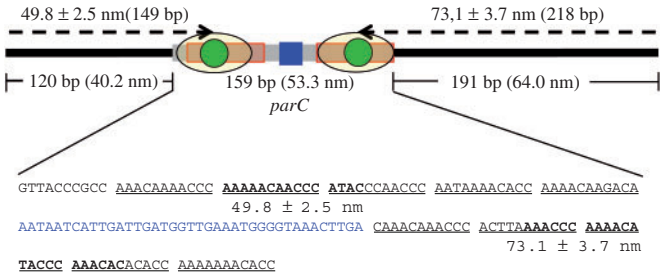

Figure 4. Localization of the complex centres. Shown is a summary of the AFM analyses in air. Black line, pKG330 DNA; grey line, *parC* site; transparent red boxes, regions of iteron repeats; green circles position of ParR complex centres in *parC*; blue box, protein-free region; dashed arrows, distances from the ParR complex centres to the tips of the nearest DNA arms; transparent yellow ovals, average size and positions of the ParR complexes. The *parC* sequence is shown at the bottom. Iteron repeats are underlined, the region between the iteron boxes is in blue font, and the regions of complex centres are marked in bold letters. Distances between the ends of fragments and centres of ParR complexes were measured (nm) while the lengths of flanking regions result from DNA sequences. The relationship between bp and nm length is given by the rise per base pair of 0.335 nm.

is ~1.5 times the DNA value (8.3 nm). For the complex length, measured along the complex contour, we assume the correction value of 5.5 nm, since the height step between DNA and protein complex is roughly the same as the step between surface and DNA. On average, the complexes were 3.5 nm high, 18.3 nm long (after subtraction of the correction value 5.5 nm) and 6.9 nm (after correction of 8.3 nm) or 9.4 nm (after correction of 5.5 nm) wide. A correction of the peak height according to data of

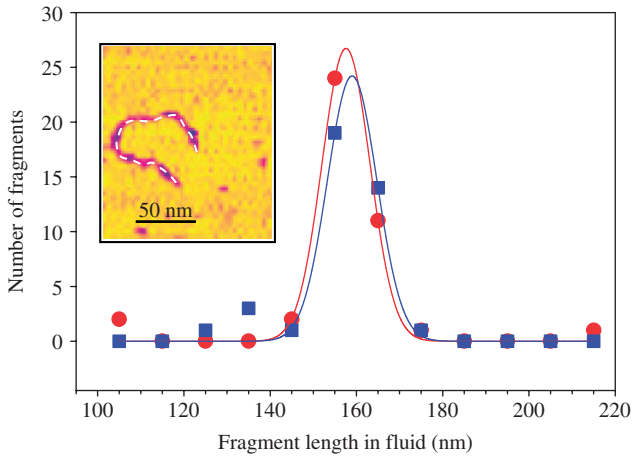

Figure 5. Comparison of lengths of naked DNA and *parC*/ParR complexes. The data result from the AFM analyses in fluid. The measured length values are symbolized by blue squares for the naked DNA and by red circles for the *parC*/ParR complexes. The Gaussian fits of these data are shown by lines in the corresponding colours. Insert shows a single naked DNA molecule resulting from a scan in fluid in the absence of ParR. White dashed line indicates the DNA contour for the distance measurements.

Bussiek *et al.* (32,33) would increase the height value from 3.5 to 4.3 nm. Assuming an ellipsoidal shape, the volume of one protein complex ($V = 4\pi abc/3$) is, after subtraction of the DNA volume (35 nm^3), 190–340 nm^3. The estimated size of the complexes clearly indicates that they contain more than one ParR molecule. When calculating the theoretical molecular volume of ParR according to protein density values (34), we obtained 7 to 12 ParR molecules in one complex. This rough estimate agrees with data of Møller-Jensen *et al.* (12) and suggests that each of the five iterons in one complex can bind about one ParR dimer.

Due to ParR binding, the DNA–protein complex displayed a folded U-shaped overall structure on the scanning surface. We analysed several aspects of this complex. First, we determined the position of the ParR complexes on the DNA in order to learn whether the ParR complexes were formed specifically at the two 5-fold repeated iteron regions on *parC*. These iterons are asymmetrically positioned on the 470 bp DNA fragment resulting in a short and a long unbound DNA end region. For a large number of complexes (~300), we determined the distances between the centres of the ParR protein peaks and the ends of the respective nearest DNA arm along the DNA contours. As a result, we obtained two clear maxima at distances of 49.8 ± 2.5 nm and 73.1 ± 3.7 nm (Figure 3). The resulting positions were almost identical for measurements under fluid (82 complexes analysed) and in air (203 complexes analysed) (Figure 3). The measured distances match the positions of the two iteron repeats within the *parC* containing DNA fragment (Figure 4). The position of the complex centre close to the short DNA arm seems to be located asymmetrically within the iteron repeats, however considering the experimental variance (2.5 nm) it still covers the iteron repeat. Moreover, the length of the complexes

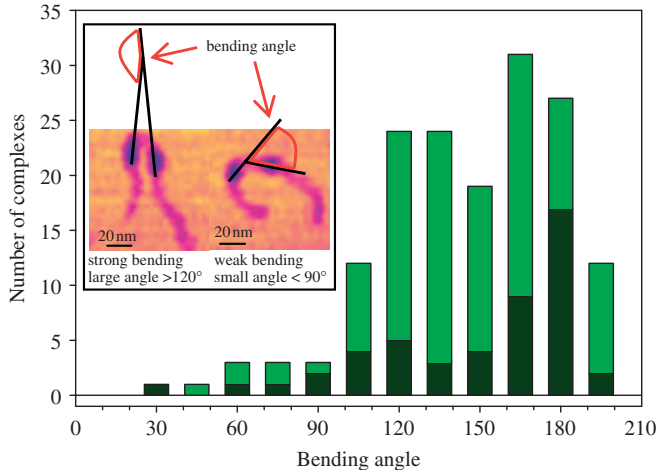

Figure 6. Analysis of bending angles in *parC*/ParR complexes. The stacked bars chart shows the distribution of bending angles analysed in fluid (dark green bars) and in air (bright green bars). Insert left, example for a complex in fluid with strong bending and large bending angle; insert right, example for a complex in fluid with weak bending and small bending angle.

(corrected value is 18.3 nm) covered the whole length of a single 5-fold iteron repeat (18.4 nm, Figure 4). Thus, ParR specifically binds the two iteron regions. We obtained the same result (i.e. two independent ParR protein peaks on the *parC* DNA fragment) also at a different buffer condition (HEPES buffer, data not shown).

We then analysed the length of the DNA fragments with bound ParR to detect any folding of the DNA within the two complexes. DNA folding in one or both ParR complexes would result in an apparent shortening of the complexed fragments. In contrast to this situation, the ParR complexed *parC* fragment length was determined to be 157.7 ± 3.9 nm (Figure 5) almost identical to the length of the naked DNA. Imaging under fluid and after air drying consistantly gave the same result (data not shown). We thus conclude that the DNA within a single complex with ParR keeps its linear path and is neither stretched nor compacted.

A visual inspection of the AFM images (Figures 2A–E and 3 (insert)) reveals that the entire complex consisting of DNA and the two ParR complexes has a hinge-like folded conformation, in such a way that the two ParR complex ends tend to point in the same direction. The structures were characterized quantitatively as follows: we connected the entry and exit points of the DNA for each ParR complex by straight lines and defined the bending angle as the angle between these two lines (see insert of Figure 6). We chose that angle which is close to zero for straight ParR-bound *parC* DNA and which becomes ~180° when the DNA folds back (Figure 6). We analysed 209 DNA fragments (49 under fluid, 160 under air) each bound by two ParR complexes, and determined the bending angle. We obtained a broad maximum of the bending angle centred at ~150°, for data measured under fluid as well as air (Figure 6). This indicates a U-shaped closely folded complex structure for the *parC*/ParR complex. A more close inspection of the broad maximum displayed a hint that the bending angle shows two distinct maxima at ~130 and 170°. An additional extensive experimental analysis would be required to prove the existence of two maxima.

In order to compare *parC* curvature with *parC*/ParR complex folding, we analysed the point-to-point distances of two defined locations on the linear DNA. For both types of DNA, *parC* in complex with ParR as well as free *parC*, we defined the two positions in a distance of 40 nm from each of the two ends of the DNA arms (Figure 2C and F). Forty nanometre is the distance from the tip of the short DNA arm to the nearest ParR complex (Figure 4). The distance between the two points within one complex reflects the strength of bending, a short distance relates to strong bending while a longer distance corresponds to weak or no bending/curvature. The mean point-to-point distance for naked *parC* was 43 nm (21 molecules analysed). This value was reduced to 23 nm when *parC* was bound to ParR (25 molecules analysed). The calculated length of the straight DNA connecting both points is 77 nm. Thus, ParR binding considerably bends *parC* beyond its intrinsic curvature.

In most *parC*/ParR complexes (we only observed a few exceptions as mentioned above), we observed two independent ParR peaks well separated on the DNA and positioned on the two 5-fold iteron repeats. We never observed dimerized ParR complexes on one *parC* DNA molecule (intramolecular) nor a dimerization between ParR complexes bound to two different *parC* DNA molecules (intermolecular). When adding glutaraldehyde to the complexation conditions, however, we noticed protein aggregation (data not shown).

DISCUSSION

Cell division must guarantee that both daughter cells will be equipped with the full set of essential genes. When the DNA is present in only a single copy or in very low copy numbers, statistical distribution of the DNA might result in genetically defective daughter cells. In order to avoid this catastrophe, cells contain active segregation machineries that grant proper DNA distribution into the daughter cells. In principle, these multiprotein–DNA complexes contain three elements: (i) a DNA localization site ('centromere'), (ii) single or many proteins recognizing this site and (iii) a force transmission element (mostly a filament). Eukaryotes contain very complex segregation machineries (kinetochores), and since here the genome is distributed over several chromosomes, segregation has to be tightly controlled which seems not to be required in prokaryotes. Since often large amounts of DNA have to be moved through viscous cellular plasma, strong complex binding is required which can be realized by many binding contacts. Consistent with this idea, kinetochores/centromeres are multiprotein–DNA complexes forming many protein–DNA contacts, with the centromeres offering preferred binding sites by being curved (21,26). These centromeric nucleosomes are particularly stable (20,35,36). Prokaryotic segregation systems were described for low-copy-number plasmids. However,

par systems are also found for bacterial chromosomes (37) although bacterial chromosome segregation seems to be mediated by multiple, overlapping or redundant mechanisms (38). We speculated, whether the prokaryotic, as the eukaryotic, centromeres also form globularly folded structures with their segregation proteins.

The *E. coli* low-copy-number plasmid R1 actively regulates its own segregation by its centromere site *parC*, its segregation protein ParR and the filament forming protein ParM (10). ParR binds to two sets of 5-fold repeated iterons separated on *parC* by 39 bp containing the *par* promoter (9,10). ParM binds to the *parC*/ParR complex, forms long stable bipolar bundles and pushes the R1 centromere to the new location (16). Applying AFM, we showed here that about 7 to 12 ParR molecules bind to each of the two 5-fold repeated iterons separately (i.e. about one ParR dimer per single 11 bp iteron) with the connecting *par* promoter sequence unbound by ParR. The protein peak centre is located close to the middle of the 5-fold repeated iteron region and the two protein complexes on *parC* do not complex with each other. The measured DNA fragment lengths were in perfect agreement with expectations for B-DNA and the contour measurements indicated that each of the two *parC* 5-fold interon DNA stretches is not compacted or shortened in its complex with ParR (in agreement with electron microscopy data of Jensen *et al*. (28)). However, the overall *parC*/ParR complex with both 5-fold iterons bound by ParR forms a folded structure: the linear DNA folds back on itself nearly completely well beyond the intrinsic *parC* curvature, including an angle of $\sim 150^{\circ}$. This can easily be explained by the joint influences of *parC* curvature together with ParR DNA bending: ParR bending in phase with the DNA curvature would result in a strong overall folding angle, a non-perfect phasing in a reduced angle. ParR-binding modes with slightly different phasing would be consistent with the indication for two folding angles (Figure 6). The functional link between curvature, binding preference and additional protein bending is difficult to analyse since modified (straight) DNA would serve as control. Straight DNA, however, would be designed by chemical or sequence modification that is expected to affect protein binding.

U-shaped structures had already been detected for the *parC*/ParR complex by electron microscopy (Figure 2B in Jensen *et al*. (28)). This structure would show an increased circularization efficiency over linear *parC* DNA and would be even further compacted by supercoiling, in agreement with experimental data (28). Our analysis resulted in a *parC*/ParR complex description of high spatial resolution. We identified the ParR binding position well within each of the two 5-fold iterons. We determined the binding location and complex structure under different buffer conditions, in liquid under buffer as well as dried under air. These high-resolution data are necessary for being able to compare the binding modes of the different par systems in detail and to deduce mechanisms for par function.

In our experiments using linear DNA, we did not observe any *parC* dimer formation mediated by ParR binding. This result is in agreement with gel shift data of Møller-Jensen *et al*. (12). However, Jensen *et al*. (28) observed some dimer formation for linear *parC* complexed with ParR. We applied higher amounts of molecules in smaller volumes compared to that study and analysed protein to DNA ratios up to 60:1 at the lower limit of those ratios (50:1 up to 500:1) applied by these authors. This dimer formation of linear DNA observed by Jensen *et al*. (28) might be due to their application of the fixation agent glutaraldehyde; in the presence of glutaraldehyde, we also detected protein aggregation. Strong dimer formation was observed by Jensen *et al*. (28) for superhelical *parC* as well as in the presence of ParM in addition to ParR, experimental conditions not studied here. Plasmid pairing is assumed to contribute to the DNA segregation mechanism (10,39–42) and it would be important to identify those molecules which are responsible for this function. Experimental evidence for the pairing hypothesis however is weak (40). Our data indicate that under our experimental conditions, plasmid pairing is not induced by linear *parC* and ParR alone, nevertheless, it might be induced by ParM and/or other factors.

Other bacterial low-copy-number plasmid segregation systems show similar properties. The P1 *E. coli* low-copy-number plasmid partition module contains the centromeric region *parS* which is recognized by ParB (6,41,43–45). The *parS* centromere itself is intrinsically curved (our unpublished data) and consists of two arms that harbour non-symmetrical hexamer and heptamer DNA motifs, separated by a central binding site for the *E. coli* integration host factor (IHF) protein (46–49). ParB is a bifunctional DNA-binding protein that recognizes both hexamer and heptamer boxes (46,47,49). IHF binding induces a pronounced bend in *parS* (by $\sim 180^{\circ}$ (50,51)), thereby positioning the ParB binding sites in the two arms (46,47,52,53). IHF-mediated bending of *parS* can be mimicked in part by an intrinsic DNA curvature that maintains the correct helical phasing of the arms resulting in $\sim$30% remaining biological activity (47). Thus, principally IHF is an architectural bending element in the *parS* segrosome. The specific P1 segrosome topology formed by *parS*, IHF and ParB in turn recruits ParA. Parallel to IHF function, *parC* is strongly curved, however, instead of ParB-binding site bridging we observed no interaction between the two ParR-binding complexes. One could speculate that, if bridging is necessary for segrosome function, this scope might be performed by ParM or another, yet unknown, plasmid or host protein. This was recently discussed for the F plasmid segregation system (54). Also the *Enterococcus faecium* segrosome, the *cenE*/PrgO complex, shows striking similarities (55): the centromere of the *E. faecium* plasmid is organized into two 7-fold DNA repeat blocks containing dTATA sequences, separated by a 26 bp intervening sequence, and displays DNA curvature to a similar amount as yeast (*S. cerevisiae*) centromeres (21), however smaller than the curvature of *parC* (26). The segregation protein PrgO binds independently to the two DNA dTATA repeats (55). The *E. faecium* segregation complex, however, remains rather straight and does not fold back on itself into a U-shaped form as *parC*/ParR and *parS*/IHF/ParB. As *parC*/ParR, also the *E. faecium cenE*/PrgO

complex shows no dimerization, neither inter- nor intramolecular (55). Again, if stabilization of a folded back architecture would be necessary for segrosome function, this might be performed by either the ParA homologue, PrgP, or another, yet unknown, plasmid or host protein. This leads to the speculation that the partition complexes might have a similar overall structural organization and, at least in part, common functional properties. It will be interesting to analyse if these similar elements are of a general nature.

ACKNOWLEDGEMENTS

We thank S. Pfeiffer and R. Klimitsch for excellent technical support.

Conflict of interest statement. None declared.

REFERENCES

1. Hayes,F. (2003) Toxin-antitoxins: plasmid maintenance, programmed cell death, and cell cycle arrest. *Science*, **301**, 1496–1499.
2. Hiraga,S. (2000) Dynamic localization of bacterial and plasmid chromosomes. *Annu. Rev. Genet.*, **34**, 21–59.
3. Gordon,G.S. and Wright,A. (2000) DNA segregation in bacteria. *Annu. Rev. Microbiol.*, **54**, 681–708.
4. Møller-Jensen,J., Jensen,R.B. and Gerdes,K. (2000) Plasmid and chromosome segregation in prokaryotes. *Trends Microbiol.*, **8**, 313–320.
5. Pogliano,J. (2002) Dynamic cellular location of bacterial plasmids. *Curr. Opin. Microbiol.*, **5**, 586–590.
6. Hayes,F. and Barillà,D. (2006) The bacterial segrosome: a dynamic nucleoprotein machine for DNA trafficking and segregation. *Nat. Rev. Microbiol.*, **4**, 133–143.
7. Gerdes,K. and Molin,S. (1986) Partitioning of plasmid R1: structural and functional analysis of the parA locus. *J. Mol. Biol.*, **190**, 269–279.
8. Møller-Jensen,J., Jensen,R.B., Lowe,J. and Gerdes,K. (2002) Prokaryotic DNA segregation by an actin-like filament. *EMBO J.*, **21**, 3119–3127.
9. Dam,M. and Gerdes,K. (1994) Partitioning of plasmid R1. Ten direct repeats flanking the parA promoter constitute a centromere-like partition site *parC*, that expresses incompatibility. *J. Mol. Biol.*, **236**, 1289–1298.
10. Jensen,R.B., Dam,M. and Gerdes,K. (1994) Partitioning of plasmid R1. The parA operon is autoregulated by ParR and its transcription is highly stimulated by a downstream activating element. *J. Mol. Biol.*, **236**, 1299–1309.
11. Breuner,A., Jensen,R.B., Dam,M., Pedersen,S. and Gerdes,K. (1996) The centromere-like parC locus of plasmid R1. *Mol. Microbiol.*, **20**, 581–592.
12. Møller-Jensen,J., Borch,J., Dam,M., Jensen,R.B., Roepstorff,P. and Gerdes,K. (2003) Bacterial mitosis: parM of plasmid R1 moves plasmid DNA by an actin-like insertional polymerization mechanism. *Mol. Cell*, **12**, 1477–1487.
13. Bork,P., Sander,C. and Valencia,A. (1992) An ATPase domain common to prokaryotic cell cycle proteins, sugar kinases, actin, and heat shock proteins. *Proc. Natl Acad. Sci. USA*, **89**, 7290–7294.
14. Gerdes,K., Møller-Jensen,J. and Jensen,R.B. (2000) Plasmid and chromosome partitioning: surprises from phylogeny. *Mol. Microbiol.*, **37**, 455–466.
15. Garner,E.C., Campbell,C.S. and Mullins,R.D. (2004) Dynamic instability in a DNA-segregating prokaryotic actin homolog. *Science*, **306**, 1021–1025.
16. Garner,E.C., Campbell,C.S., Weibel,D.B. and Mullins,R.D. (2007) Reconstitution of DNA segregation driven by assembly of a prokaryotic actin homolog. *Science*, **315**, 1270–1274.
17. van den Ent,F., Møller-Jensen,J., Amos,L.A., Gerdes,K. and Löwe,J. (2002) F-actin-like filaments formed by plasmid segregation protein ParM. *EMBO J.*, **21**, 1–9.
18. Mestrovic,N., Mravinac,B., Juan,C., Ugarkovic,D. and Plohl,M. (2000) Comparative study of satellite sequences and phylogeny of five species from the genus Palorus (Insecta, Coleoptera). *Genome*, **43**, 776–785.
19. Fitzgerald,D.J., Dryden,G.L., Bronson,E.C., Williams,J.S. and Anderson,J.N. (1994) Conserved patterns of bending in satellite and nucleosome positioning DNA. *J. Biol. Chem.*, **269**, 21303–21314.
20. Segal,E., Fondufe-Mittendorf,Y., Chen,L., Thaström,A., Field,Y., Moore,I.K., Wang,J.-P. and Widom,J. (2006) A genomic code for nucleosome positioning. *Nature*, **442**, 750–752.
21. Bechert,T., Heck,S., Fleig,U., Diekmann,S. and Hegemann,J.H. (1999) All 16 centromere DNAs of *Saccharomyces cerevisiae* show DNA curvature. *Nucleic Acids Res.*, **27**, 1444–1449.
22. Wu,H.M. and Crothers,D.M. (1984) The locus of sequence-directed and protein-induced DNA bending. *Nature*, **308**, 509–513.
23. Diekmann,S. and Wang,J.C. (1985) On the sequence determinants and flexibility of the kinetoplast DNA fragment with abnormal gel electrophoretic mobilities. *J. Mol. Biol.*, **186**, 1–11.
24. Diekmann,S. (1987) Temperature and salt dependence of the gel migration anomaly of curved DNA fragments. *Nucleic Acids Res.*, **15**, 247–265.
25. Koo,H.S., Wu,H.M. and Crothers,D.M. (1986) DNA bending at adenine:thymine tracts. *Nature*, **320**, 501–506.
26. Hoischen,C., Bolshoy,A., Gerdes,K. and Diekmann,S. (2004) Centromere parC of plasmid R1 is curved. *Nucleic Acids Res.*, **32**, 5907–5915.
27. Nordström,K. and Austin,S.J. (1989) Mechanisms that contribute to the stable segregation of plasmids. *Annu. Rev. Genet.*, **23**, 37–69.
28. Jensen,R.B., Lurz,R. and Gerdes,K. (1998) Mechanism of DNA segregation in prokaryotes: replicon pairing by *parC* of plasmid R1. *Proc. Natl Acad. Sci. USA*, **95**, 8550–8555.
29. Ausubel,F.M., Brent,R., Kingston,R.E., Moore,D.D., Seidman,J.G., Smith,J.A. and Struhl,K. (eds). (1994) *Current Protocols in Molecular Biology*. John Wiley and Sons, NY.
30. Bussiek,M., Mucke,N. and Langowski,J. (2003) Polylysine-coated mica can be used to observe systematic changes in the supercoiled DNA conformation by scanning force microscopy in solution. *Nucleic Acids Res.*, **31**, e137.
31. Rippe,K., Mücke,N. and Langowski,J. (1997) Superhelix dimensions of a 1868 base pair plasmid determined by scanning force microscopy in air and in aqueous solution. *Nucleic Acids Res.*, **25**, 1736–1744.
32. Bussiek,M., Toth,K., Brun,N. and Langowski,J. (2005) DNA-loop formation on nucleosomes shown by *in situ* scanning force microscopy of supercoiled DNA. *J. Mol. Biol.*, **345**, 695–706.
33. Bussiek,M., Muller,G., Waldeck,W., Diekmann,S. and Langowski,J. (2007) Organisation of nucleosomal arrays reconstituted with repetitive African green monkey alpha-satellite DNA as analysed by atomic force microscopy. *Eur. Biophys. J.*, 15 May 2007 [Epub ahead of print].
34. Pietrasanta,L.I., Thrower,D., Hsieh,W., Rao,S., Stemmann,O., Lechner,J., Carbon,J. and Hansma,H. (1999) Probing the *Saccharomyces cerevisiae* centromeric DNA (*CEN* DNA)-binding factor 3 (CBF3) kinetochore complex by using atomic force microscopy. *Proc. Natl Acad. Sci. USA*, **96**, 3757–3762.
35. Amor,D.J., Kalitsis,P., Sumer,H. and Choo,K.H.A. (2004) Building the centromere: from foundation proteins to 3D organisation. *Trends Cell Biol.*, **14**, 359–368.
36. Black,B.E., Foltz,D.R., Chakravarthy,S., Luger,K., Woods,V.L. and Cleveland,D.W. (2004) Structural determinants for generating centromeric chromatin. *Nature*, **430**, 578–582.
37. Fogel,M.A. and Waldor,M.K. (2007) A dynamic, mitotic-like mechanism for bacterial chromosome segregation. *Genes & Dev.*, **20**, 3269–3282.
38. Errington,J., Murray,H. and Wu,L.J. (2005) Diversisty and redundancy in bacterial chromosome segregation mechanisms. *Phil. Trans. R. Soc. Lond. B Biol. Sci.*, **360**, 497–505.
39. Lin,D.C. and Grossman,A.D. (1998) Identification and characterization of a bacterial chromosome partitioning site. *Cell*, **92**, 675–685.
40. Edgar,E., Chattoraj,D.K. and Yarmolinsky,M. (2001) Pairing of P1 plasmid partition sites by ParB. *Mol. Microbiol.*, **42**, 1363–1370.

41. Schumacher,M.A. (2007) Structural biology of plasmid segregation proteins. *Curr. Opin. Struct. Biol.*, **17**, 103–109.
42. Funnell,B.E. (2005) Partition-mediated plasmid pairing. *Plasmid*, **53**, 119–125.
43. Schumacher,M.A. and Funnell,B.E. (2005) Structures of ParB bound to DNA reveal mechanism of partition complex formation. *Nature*, **438**, 516–519.
44. Schumacher,M.A., Mansoor,A. and Funnell,B.E. (2007) Structure of a four-way bridged parB-DNA complex provides insight into P1 segrosome assembly. *J. Biol. Chem.*, **282**, 10456–10464.
45. Vecchiarelli,A.G., Schumacher,M.A. and Funnell,B.E. (2007) P1 partition complex assembly involves several modes of protein-DNA-recognition. *J. Biol. Chem.*, **282**, 10944–10952.
46. Davis,M.A. and Austin,S. (1988) Recognition of the P1 plasmid centromere analog involves binding of the ParB protein and is modified by a specific host factor. *EMBO J.*, **7**, 1881–1888.
47. Hayes,F. and Austin,S. (1994) Topological scanning of the P1 plasmid partition site. *J. Mol. Biol.*, **243**, 190–198.
48. Martin,K.A., Davis,M.A. and Austin,S.J. (1991) Fine structure analysis of the P1 plasmid partition site. *J. Bacteriol.*, **173**, 3630–3634.
49. Surtees,J.A. and Funnell,B.E. (2001) The DNA binding domains of P1 ParB and the architecture of the P1 plasmid partition complex. *J. Biol. Chem.*, **276**, 12385–12394.
50. Rice,P.A., Yang,S., Mizuuchi,K. and Nash,H.A. (1996) Crystal structure of an IHF-DNA complex: a protein-induced DNA U-turn. *Cell*, **87**, 1295–1306.
51. Lorenz,M., Hillsich,A., Goodman,S.D. and Diekmann,S. (1999) Global structure similarities of intact and nicked DNA complexed with IHF measured in solution by FRET. *Nucleic Acids Res.*, **27**, 4619–4625.
52. Funnell,B.E. (1988) Participation of *E. coli* integration host factor in the P1 plasmid partition system. *Proc. Natl Acad. Sci. USA*, **85**, 6657–6661.
53. Funnell,B.E. (1991) The P1 plasmid partition complex at *parS*. The influence of *E. coli* integration host factor and of substrate topology. *J. Biol. Chem.*, **266**, 14328–14337.
54. Bouet,J.Y., Bouvier,M. and Lane,D. (2006) Concerted action of plasmid maintenance functions: partition complexes create a requirement for dimer resolution. *Mol. Microbiol.*, **62**, 1447–1459.
55. Derome,A., Hoischen,C., Grady,R., Kędzierska,B., Bussiek,M., Diekmann,S., Daniela Barillà,D. and Hayes,F. (2007) Centromere anatomy in the multidrug resistant pathogen. *Enterococcus faecium*, submitted.